IEEE Access
Multidisciplinary | Rapid Review | Open Access Journal

SPECIAL SECTION ON DATA-DRIVEN MONITORING, FAULT DIAGNOSIS AND CONTROL OF CYBER-PHYSICAL SYSTEMS

Received November 8, 2017, accepted December 10, 2017, date of publication December 13, 2017,
date of current version March 9, 2018.

Digital Object Identifier 10.1109/ACCESS.2017.2782879

Hybrid Prediction Method for the Electromagnetic Interference Characteristics of Printed Circuit Boards Based on the Equivalent Dipole Model and the Finite-Difference Time Domain Method

LANYONG ZHANG[1,2,3], (Member, IEEE), LEI ZHANG[1], (Member, IEEE), BANGMIN WANG[1], SHENG LIU[1], AND CHRISTOS PAPAVASSILIOU[2], (Senior Member, IEEE)

[1]College of Automation, Harbin Engineering University, Harbin 150001, China
[2]Department of Electrical and Electronic Engineering, Imperial College London, London SW7 2AZ, U.K.
[3]State Key Laboratory of Millimeter Waves, Nanjing 210096, China

Corresponding author: Lanyong Zhang (zlyalf@sina.com)

This work was supported in part by the National Natural Science Foundation of China subsidization project under Grant 51579047, in part by the Natural Science Foundation of Heilongjiang Province under Grant QC2017048, in part by the National Defense Technology Fundamental Research Funds under Grant JSHS2015604C002, in part by the Natural Science Foundation of Harbin under Grant 2016RAQXJ077, and in part by the Open Project Program of State Key Laboratory of Millimeter Waves under Grant K201707.

ABSTRACT In this paper, we propose a hybrid modeling method for analyzing the electromagnetic compatibility characteristics of printed circuit boards (PCBs). The method uses an equivalent magnetic dipole array deduced from near-field scanning results obtained at a certain height over the PCB surface under test and the finite-difference time domain (FDTD) algorithm. The array of dipoles can simulate the PCB electromagnetic emissions, including the ground plane effect at a particular high frequency; the equivalent dipole array can then be imported into the FDTD calculation space for calculating the electromagnetic fields generated by the dipole array. In our experiment, we obtained the tangential magnetic field distribution of the PCB surface using near-field scanning, from where the tangential magnetic field component, orientation, and the magnitude and phase of the dipoles could be deduced. We used the proposed method to model two different modules on a highly integrated circuit. The results of the proposed method and those obtained by near-field scanning are nearly the same, which demonstrates the effectiveness and accuracy of the proposed method. We therefore conclude that the proposed modeling approach presents a new technique for studying the electromagnetic interference of PCBs.

INDEX TERMS Electromagnetic compatibility, equivalent dipole model, finite-difference time domain, printed circuit board.

I. INTRODUCTION

Printed circuit boards (PCBs) are important components of electronic devices. With the development of integrated circuits, a PCB can include many highly integrated active chips, passive lumped elements, and package structures. The resulting increase in signal frequency, clock frequency, and circuit configuration complexity causes serious coupling phenomena. When electronic devices operate at megahertz frequencies or higher, the involved circuits become electromagnetic radiation sources, and the radio frequency (RF) interference produced by such high-frequency circuits can cause many electromagnetic compatibility (EMC) problems. The devices' EMC characteristics must be properly considered, both in the design phase and in the subsequent engineering applications.

There have been some studies on far-field electromagnetic interference (EMI) prediction models. In [1], a modal expansion method is used to construct a model of the radiation sources, whereas in [2] the EMI is modeled using an equivalent current and magnetic current model. A Huygens equivalent source has also been used to construct the EMC model [3]. These three approaches focus on far-field radiation

prediction; therefore, the interaction between the radiation source and objects in its close vicinity cannot be correctly described.

Good results have been achieved by using equivalent dipole models to study PCB EMC characteristics. The equivalent dipole modeling method has been successfully used to construct the EMI model of a PCB and its embedded components [4], [5]. Near-field scanning technology has been combined with the equivalent dipole model, and it was found that only the tangential magnetic components are needed to construct an equivalent model of the chips and micro-strip lines [6]. Moreover, this model can consist of either electric dipoles or magnetic dipoles, and shows the EMI distribution for a given working frequency. Both [7] and [8] propose equivalent models in the time domain using near-field scanning technology and equivalent electric dipoles; these models can present the radiation characteristics of the PCB under test in the time domain. Compared with the equivalent magnetic dipole model in the frequency domain, the time domain equivalent model has higher prediction accuracy, but the modeling process is more complex and time consuming.

In [9], a duplication-degeneration-complementation approach to build an equivalent PCB model-including the ground plane-was proposed. The reciprocity theorem has also been used to estimate radio-frequency interference in a PCB [10]; this method can be used to obtain the distribution of the near-field magnetic and electric components on the Huygens surface, from which the equivalent dipole moment model can be deduced.

In addition to the equivalent dipole modeling method, the finite-difference time domain (FDTD) method has also been widely used in the study of the EMC characteristics of some devices. The FDTD algorithm is a computational electromagnetics solver that discretizes the Maxwell's equations in a form convenient for obtaining the numerical solution of field problems involving complex three-dimensional objects of arbitrary shapes and arbitrary material characteristics. The FDTD method (and its calculation performance) has been improved in many different ways. The set of improved FDTD methods includes the alternating direction implicit FDTD method [11], [12], the locally one-dimensional FDTD scheme [13], [14], and the J electromagnetic solver FDTD (JEMS-FDTD) method [15]. The calculation boundary has also been improved [16]–[18].

Hikage *et al.* [19] presented an FDTD method for analyzing the EMI caused by a radio-frequency identification interrogator in an active implantable medical device. A hybrid method for analyzing the EMI of lumped circuits in shielded devices has been presented in [20], which includes both the FDTD method with transmission line equations and a circuit-based method. Finally, an FDTD-based analysis of the EMI produced by the insulated-gate bipolar transistor (IGBT) in a motor drive system has been demonstrated in [21].

In this study, we propose a novel hybrid modeling method based on the equivalent dipole method and the FDTD algorithm, which can be directly used in the time domain to model the EMI generated by PCBs under different working conditions. The modeling method can be divided in two parts: the first part builds the equivalent magnetic dipole model of the microstrip lines, components, dielectric layers, and ground plane, whereas the second part calculates the model in the FDTD calculation space with uniaxial perfectly matched layers (UPML) as boundary conditions; the combination of both methods is effective in predicting the EMI generated by the PCB. Furthermore, the proposed algorithm uses equivalent magnetic dipole array deduced from near field scanning results and the FDTD algorithm to predict far-field radiation, even substitute the PCB to investigate the interactions between the PCB and the surroundings such as the shielding cavity. The conventional equivalent dipole modeling method is used to model the equivalent dipole parameters through near-field scan data and then calculate the space electromagnetic field directly through these parameters.The method proposed in this paper is to reconstruct the space electromagnetic field through the FDTD after the equivalent dipole parameter is obtained. The advantages of this method are simple and accurate. On the other hand, it is convenient to establish the interaction between the model and the interference source.

The remainder of this paper is organized as follows. The theory underlying the proposed method is introduced in Section II. In Section III, the proposed hybrid method is demonstrated in two study cases, and the potential of this method for the EMI protection of a shielded electronic device is verified. The obtained results are discussed in Section IV. Section V presents some final conclusions.

II. HYBRID MODELING METHOD THEORY

A. EQUIVALENT DIPOLE MODELING THEORY

In this subsection, we will discuss how to obtain the equivalent dipoles. Based on the equivalence principle (i.e., the equivalent dipoles should radiate the same field as the actual PCB), the moment and orientation of the dipoles can be determined by solving the inverse problem of matching the measurement results obtained by near-field scanning. Subsequently, we will discuss in detail how to produce the full equivalent dipole model.

In equivalent dipole modeling, the PCB is replaced with an array of infinitesimal electric or magnetic equivalent dipoles placed on a perfect electrically conducting plane. The emission radiated by the equivalent dipole array approximates the real PCB electromagnetic emissions. Usually, we do not need to know the physical structure or the exact geometric dimensions of the PCB to use the equivalent dipole modeling method, given that the thickness of a PCB is very small. The array of oriented electric or magnetic dipoles placed on a plane (x-y plane) can be used to equivalently replace the PCB, as shown in Fig. 1.

The magnitude, phase, and orientation of the electric or magnetic dipoles can be determined by the magnetic components $H_x(A/m)$, $H_y(A/m)$, and $H_z(A/m)$, which can be obtained from near-field scanning the PCB surface.

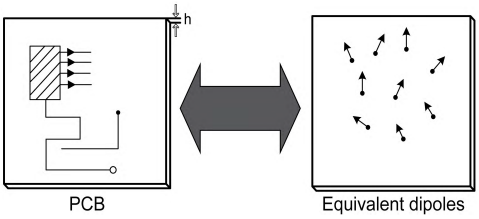

FIGURE 1. Equivalent dipole model.

Let us consider the magnetic field generated by a single magnetic dipole. A magnetic dipole can be represented by a closed current-carrying conductor with radius a and current $I_0(A)$. Suppose that a finite small magnetic dipole $M(A·H·m)$ is placed at (x_0, y_0, z_0), oriented in the z direction. Let $R(m)$ be the distance between the magnetic dipole and an observation point (x, y, z). In spherical coordinates, the magnetic field at the observation point can be expressed as follows (k being the wavenumber corresponding to wavelength λ; $k(m^{-1}) = 2\pi/\lambda$):

$$H(r) = \frac{j\omega\mu_0 I_0 \pi a^2 e^{-jkR}}{2\pi\eta_0 R^2}\cos\theta\left[1+\frac{1}{jkR}\right]a_r - \frac{\omega\mu_0 I_0\pi a^2 k e^{-jkR}}{4\pi\eta_0 R}\sin\theta\left[1+\frac{1}{jkR}-\frac{1}{k^2R^2}\right]a_\theta \quad (1)$$

where η_0 is the wave impedance in free space ($\eta_0 = \sqrt{\mu_0/\varepsilon_0}$); μ_0 and ε_0 denote the electrical permittivity and magnetic permeability of free space, respectively. The magnetic field component in the ϕ direction is zero. The magnetic field can be expressed in terms of the magnetic dipole moment $M = \mu_0 I_0 \pi a^2$ as follows:

$$H(r) = \frac{j\omega M e^{-jkR}}{2\pi\eta_0 R^2}\cos\theta\left[1+\frac{1}{jkR}\right]a_r - \frac{\omega M k R e^{-jkR}}{4\pi\eta_0 R^2}\sin\theta\left[1+\frac{1}{jkR}-\frac{1}{k^2R^2}\right]a_\theta \quad (2)$$

The magnetic dipole moment M can be divided into three components in the Cartesian coordinate system: M_x, M_y, and M_z. The magnetic field produced by M_x at the observation point (x, y, z) can be expressed as:

$$H_x = M_x\frac{jk^2e^{-jkR}(x-x_0)^2}{4\pi R^3}\left(\frac{3}{kR}+\frac{3}{jk^2R^2}+j\right) - M_x\frac{jk^2e^{-jkR}}{4\pi R}\left(j+\frac{1}{kR}+\frac{1}{jk^2R^2}\right) = \alpha_x^{x'}M_x \quad (3)$$

$$H_y = M_x\frac{jk(x-x_0)(y-y_0)}{4\pi R^4}e^{-jkR}\times\left(3+\frac{3}{jkR}+jkR\right) = \alpha_y^{x'}M_x \quad (4)$$

$$H_z = M_x\frac{jk(x-x_0)(z-z_0)}{4\pi R^4}e^{-jkR}\times\left(3+\frac{3}{jkR}+jkR\right) = \alpha_z^{x'}M_x \quad (5)$$

In equations(3)-(5), the distance between the observation point and the magnetic dipole is as follows:

$$R = \sqrt{(x-x_0)^2+(y-y_0)^2+(z-z_0)^2} \quad (6)$$

The magnetic field produced by M_y and M_z can be calculated using the same method. Consequently, we can formulate the relationship between the magnetic field H and the dipole moment M as follows:

$$\begin{bmatrix}H_x\\H_y\\H_z\end{bmatrix} = \begin{bmatrix}\alpha_x^{x'} & \alpha_x^{y'} & \alpha_x^{z'}\\ \alpha_y^{x'} & \alpha_y^{y'} & \alpha_x^{z'}\\ \alpha_z^{x'} & \alpha_z^{y'} & \alpha_z^{z'}\end{bmatrix}\begin{bmatrix}M_x\\M_y\\M_z\end{bmatrix} \quad (7)$$

In (7), the superscript and subscript of the α coefficients represent the dipole and magnetic field components, respectively. In order to establish an integrated equivalent dipole model, it is first necessary to obtain an expression of the magnetic field of the element magnetic dipole (x_0, y_0, z_0) with a surface $S(m^2)$ and current intensity of I_0, with a fixed direction, a number and a position. The magnetic field generated by this dipole can be expressed as follows:

$$H_x = \frac{jSkI_0(x-x_0)(z-z_0)}{4\pi R^4}e^{-jkR}\times\left(3+\frac{3}{jkR}+jkR\right) = \alpha_x I_0 \quad (8)$$

$$H_y = \frac{jSkI_0(y-y_0)(z-z_0)}{4\pi R^4}e^{-jkR}\times\left(3+\frac{3}{jkR}+jkR\right) = \alpha_y I_0 \quad (9)$$

$$H_z = \frac{jSk^2I_0(z-z_0)^2}{4\pi R^3}e^{-jkR}\left(\frac{3}{kR}+\frac{3}{jk^2R^2}+j\right) - \frac{jSk^2I_0}{4\pi R}e^{-jkR}\left(j+\frac{1}{kR}+\frac{1}{jk^2R^2}\right) = \alpha_z I_0 \quad (10)$$

In (8)-(10), S is the area of the magnetic dipole, which is determined by the size of the Yee cell (Discretized using a Cartesian mesh with circulating electric and magnetic field components, known as the Yee-cell) in the calculation space. While building the equivalent model, the number of observation points is m, and the number of magnetic dipoles is n. The magnetic field at every observation point is the superposition of the magnetic fields produced by every dipole. The three magnetic field components can be expressed in matrix form as follows:

$$[\alpha_x]_{m\times n}[I_0]_{n\times 1} = [H_x]_{m\times 1} \quad (11)$$

$$[\alpha_y]_{m\times n}[I_0]_{n\times 1} = [H_y]_{m\times 1} \quad (12)$$

$$[\alpha_z]_{m\times n}[I_0]_{n\times 1} = [H_z]_{m\times 1} \quad (13)$$

Solving the inverse problem in (11)-(13), the moment and current in each dipole can be determined. To obtain a unique solution matrix, the number of dipoles must be smaller than the number of observation points ($n < m$), and the dipoles and observation points cannot be in the same positions. In practice, however, the number of dipoles n is far smaller than the number of observation points m (i.e., $n < m$), leading to an

overdetermined system of equations. Therefore, conventional techniques such as Gaussian elimination cannot be applied to solve this inverse problem. Instead, a more robust technique (e.g., singular value decomposition, which is often used to solve linear least squares problems) is required to solve this ill-posed, near singular inverse problem, and obtain the desired matrix solution.

The effect of the ground plane must also be considered. As shown in [6], when the PCB is placed on the ground plane(The ground plane is a perfectly electric conductor (PEC), which can reflect radiation and influence the results of the near-field scanning), the radiation effect under the ground plane is relatively small. Usually, the ground plane is contained in the equivalent dipole model. In such a modeling method, magnetic dipoles are placed in an area smaller than the size of the PCB under test, and a mirror imaging approach is used; the effect of diffraction of the finite ground plane is ignored, and the ground plane is treated as an infinite perfectly conducting plane. Therefore, PCBs with a ground plane can be regarded as an array of dipoles placed on a perfectly conducting plane.

Using this approximation (assuming that the ground plane is infinite), the equivalent dipole model-including the ground plane-can be defined as follows:

$$[\alpha_x]_{m\times n}[I_0]_{n\times 1} + [\alpha'_x]_{m\times n}[I_0]_{n\times 1} = [H_x]_{m\times 1} \quad (14)$$

$$[\alpha_y]_{m\times n}[I_0]_{n\times 1} + [\alpha'_y]_{m\times n}[I_0]_{n\times 1} = [H_y]_{m\times 1} \quad (15)$$

$$[\alpha_z]_{m\times n}[I_0]_{n\times 1} + [\alpha'_z]_{m\times n}[I_0]_{n\times 1} = [H_z]_{m\times 1} \quad (16)$$

In equations (14)-(16), the second term on the left is the contribution of the image dipoles. In particular, it should be noted that, because the image of a magnetic dipole has the opposite current direction, it is implicitly included in this coefficient calculation procedure. We need to perform near-field scanning on a certain plane above the PCB, on which the electromagnetic fields can be measured accurately, to determine the magnetic field of the equivalent model.

B. NEAR-FIELD SCANNING PROCESS

Fig. 2 shows the near-field measuring system used to characterize the PCB under test. For simplicity, due to the near-field scanning method similarity to that in [1], we will not attempt to introduce this procedure in detail here. There needs to be pointed out that network analyzer can be applied to measure, however, compared with the spectrum analyzer, network analyzer in the treatment of stable signal, has the high level, without spurs. Unfortunately, these requirements cannot be implemented, so the spectrum analyzer is used here. The purpose of near-field scanning is to acquire the information required to produce the matrix of equivalent dipoles. The measuring height above the PCB surface is designated by h, and the PCB plane is taken as the reference plane. There are two standardized electric field probes: the measuring probe and the reference probe. In the near-field scanning process, the reference probe is held fixed on the PCB plane, while the measuring probe is moved on the scanning plane. The signal

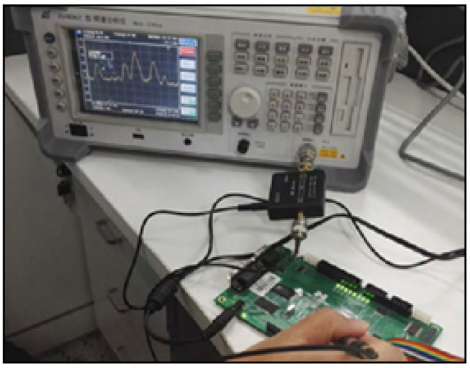

FIGURE 2. Near-field scanning procedure.

collected by the probes is transmitted to a spectrum analyzer. By measuring m discrete points, we obtain the magnetic component matrices H_x, H_y, and H_z.

The probe damping at 112.51 MHz is 45 dB, and the cable loss is 1 dB. The PCB surface voltage measured by the probe can be transformed into the form of an electric field, as follows:

$$E_{radiation} = U_{radiation} + R_{probe} + L_{loss} \quad (17)$$

Here, $E_{radiation}(dB\mu V/m)$ stands for the radiating electric field, $U_{radiation}(dB\mu V)$ represents the voltage values measured with the spectrum analyzer, $R_{probe}(dBm^{-1})$ is the probe damping, and $L_{loss}(dB)$ is the cable loss. All the elements in (17) are expressed in logarithmic form. In this study, we use the magnetic field components over the PCB surface to calculate the electric field in the far-field region; the relationship between the two fields can be calculated by electrostatic bonding theory [22], as follows:

$$H = \frac{1}{\eta}E \quad (18)$$

where $\eta(\Omega) = \sqrt{\mu_0/\varepsilon_0}$ is the wave impedance, μ_0 is the permeability, and ε_0 is the permittivity. All parameters are set considering free space conditions. By contrast, the relationship between the magnetic field and the electric field in the near-field region is relatively complicated. Fortunately, the magnetic field generated by the equivalent dipoles is the linear superposition of the magnetic fields radiated by each elementary magnetic dipole. Consequently, we can obtain the magnetic field with the following equation:

$$\nabla \times E = -j\omega\mu_0 H \quad (19)$$

where E is a phasor with the amplitude and phase measured by near-field scanning, and μ_0 is the magnetic permeability, as before. Using (17)-(19), we can obtain the magnetic field by measuring the electric field over the PCB surface. The parameters of each magnetic dipole can be deduced with the above equations.

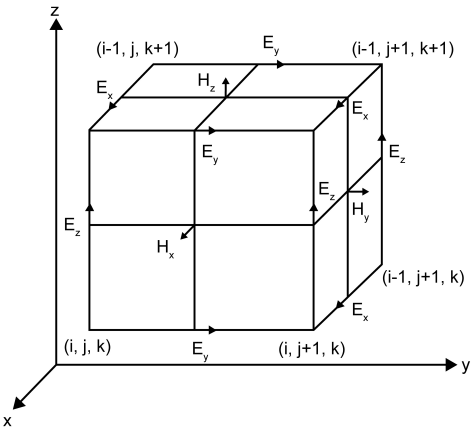

FIGURE 3. Component distribution in a Yee cell.

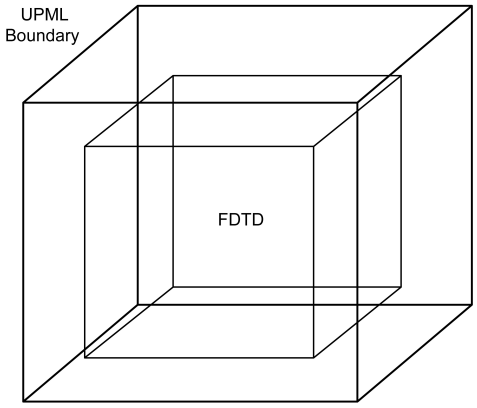

FIGURE 4. Diagram of the FDTD space and UPML.

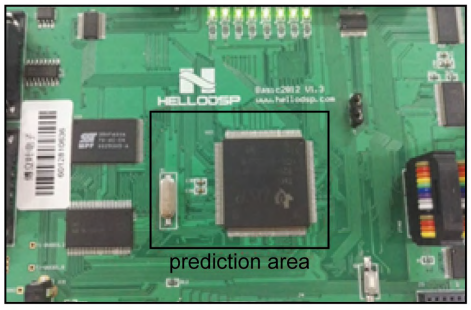

FIGURE 5. PCB structure and the prediction area 1.

C. CALCULATION OF THE EQUIVALENT DIPOLE MODEL USING THE FDTD METHOD

The FDTD algorithm is used to calculate the electromagnetic field generated by the equivalent dipole model. The calculation space is discretized as a mesh of Yee cells. The distribution of the electromagnetic field components in the Yee cell is shown in Fig. 3. Here, although the dipole radiation in free space can be easily calculated by its radiation equation, FDTD is required to obtain dipole radiation for two reasons: on the one hand, the calculation based on its radiation equations is reasonably complex and time consuming with the increasing number of observation points; on the other hand, the FDTD algorithm as an effective and efficient method can be easily exploited to character the EMI of PCB with presence of the shielding cavity.

The calculation space is considered to be free space, and the permittivity and permeability are therefore set as:

$$\varepsilon = \varepsilon_0 = 8.854 \times 10^{-12} F/m, \mu = \mu_0 = 4\pi \times 10^{-7} H/m$$

To satisfy the stability conditions and the numerical dispersion conditions of the FDTD algorithm, the proper time and space steps must be chosen. The Yee cells in the FDTD calculation space are set as regular hexahedrons. Considering the PCB area involved in the prediction, the spatial steps can be set as follows: $\triangle x = \triangle y = \triangle z = \delta = 0.5mm$. The simulation frequency is $f = 112.51\ MHz$, and the corresponding wavelength in free space is $\lambda = c/f = 3 \times 10^8/(112.51 \times 10^6) = 2.67\ m$; therefore, the numerical dispersion condition is satisfied.

Considering the stability condition of the FDTD method in free space $\triangle t \leq 1/(c\sqrt{3/(\delta)^2})$, the time step can be chosen as $t = \delta/2c = 8 \times 10^{-13} s$. The temporal and spatial spacing used in the calculation were chosen as follows: the spatial spacing is determined by the PCB size and the number of scanned points; the time spacing is determined by the sampling period of the spectrum analyzer. The excitation source is Gaussian.

The UPML boundary conditions have some advantages over other boundary conditions, such as perfectly matched layers (PMLs), Mur, and convolutional PMLs. In this study, the FDTD calculation space is surrounded by the UPML boundary, as shown in Fig. 4. The UPML thickness is 10 Yee cells.

It is important to properly set the parameters-such as the permittivity and permeability-in the overlapping areas of the UPML. The equivalent dipole model can then be imported into the calculation space, as shown in Fig. 4. The analysis of the equivalent dipole model calculation results obtained for different areas of the PCB is presented in the next section.

III. MODELING RESULTS USING THE HYBRID PREDICTION METHOD

Two areas on a four-layer PCB were modeled using the modeling approach presented above. The PCB structure is shown in Fig. 5; the other side of the PCB is backed on the ground plane.

The prediction area 1 was a 50 $mm \times 50\ mm$ area surrounding the control chip TMS320F2812, with its pins, strip lines, resistance, capacitance, and crystal oscillator, as shown in Fig. 5. The prediction area 2 had an area of $25\ mm \times 40\ mm$ and was centered around the power port, as is also shown in Fig. 6.

The experiments were performed under the following working conditions: the digital signal processor was producing a six-channel 35 MHz pulse width modulation (PWM)

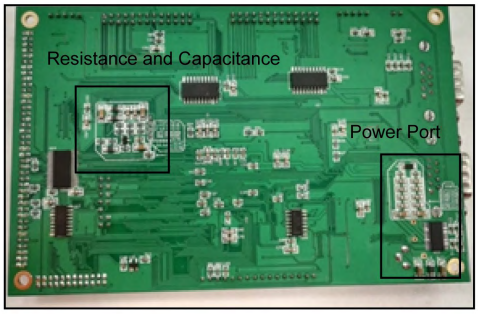

FIGURE 6. The prediction area 2 on the same PCB.

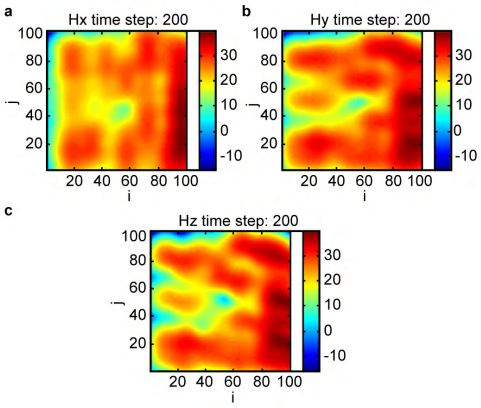

FIGURE 7. Magnetic field distribution in the area 1, calculated by the equivalent dipole model, 5 mm above the PCB surface. Magnetic field component in the (a) X direction, (b) Y direction, and (c) Z direction.

signal. In the near-field measuring process, we confirmed that the EMI generated by the areas under test reached its peak at 112.51 MHz.

Using the equations presented in the previous sections, we could obtain the equivalent dipole array, determining the orientation, magnitude, and phase of each dipole. The equivalent dipole models of the two different prediction areas were constructed using the modeling approach presented in Section II. The two resulting equivalent dipole models were then imported into the calculation space, as described in Section II. Different components of the electric and magnetic field were calculated at different heights above the PCB plane. The resulting EMI could therefore also be determined at different heights above the PCB plane.

A. PREDICTION RESULTS FOR THE PCB AREA 1

Fig. 7 and Fig. 8 show the distribution of the magnetic and electric fields over the prediction area 1, 5 *mm* above the PCB plane. In the experiment, coordinates i and j denote the horizontal and vertical axes, respectively. The magnetic field units are decibels relative to $1\mu A/m$, and the electric field units are decibels relative to $1\mu V/m$. Hereafter, the magnetic field and electric field are marked with the same unit.

Fig. 9 and Fig. 10 show the magnetic and electric field distributions for the first prediction area, 10 *mm* above the PCB plane.

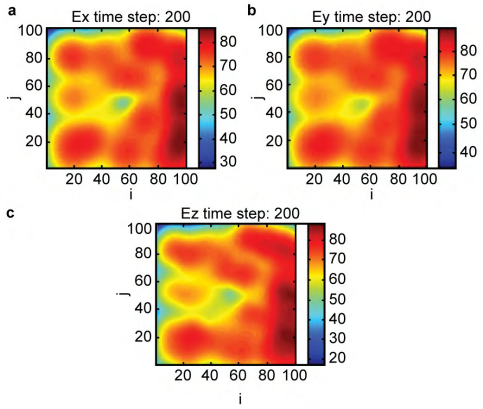

FIGURE 8. Electric field distribution in the area 1, calculated by the equivalent electric model, 5 mm above the PCB surface. Electric field component in the (a) X direction, (b) Y direction, and (c) Z direction.

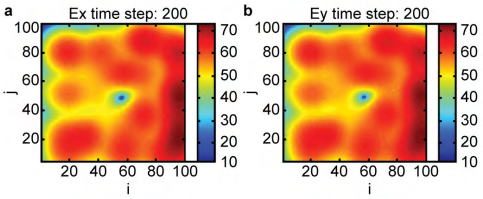

FIGURE 9. Electric field distribution in the area 1, calculated by the equivalent electric model, 10 mm above the PCB surface. Electric field component in the (a) X direction and (b) Y direction.

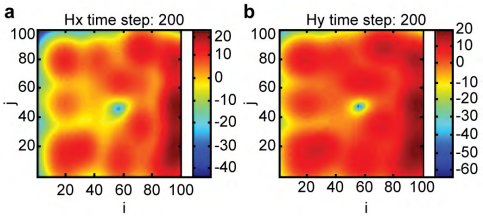

FIGURE 10. Magnetic field distribution in the area 1, calculated by the equivalent dipole model, 10 mm above the PCB surface. Magnetic field component in the (a) X direction and (b) Y direction.

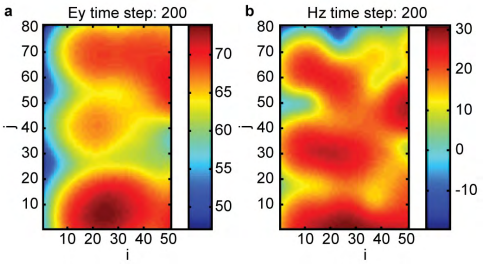

FIGURE 11. Magnetic and electric field distributions in the area 2, calculated by the equivalent dipole model, 10 mm above the PCB surface. (a) Electric field component in the Y direction. (b) Magnetic field component in the Z direction.

B. PREDICTION RESULTS FOR THE PCB AREA 2

Fig. 11 shows the magnetic and electric field distributions for the prediction area 2, 10 *mm* above the PCB plane. For brevity, we show only one component of the electric and magnetic fields.

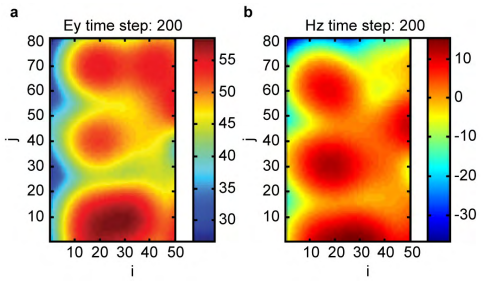

FIGURE 12. Magnetic and electric field distributions in the area 2, calculated by the equivalent dipole model, 20 mm above the PCB surface. (a) Electric field component in the Y direction. (b) Magnetic field component in the Z direction.

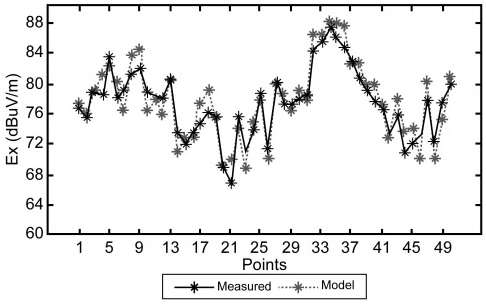

FIGURE 13. Measured and calculated results for the electric field in the area 1, 5 mm above the PCB surface.

Fig. 12 shows the magnetic and electric field distributions for the second prediction area, 20 *mm* above the PCB plane. For brevity, we show only one component of the electric and magnetic fields.

IV. VERIFICATION OF THE CALCULATED RESULTS

To validate the accuracy of the proposed hybrid prediction method-which includes the equivalent dipole model and the FDTD calculation method-we performed near-field testing, both in a general laboratory setting and in an anechoic chamber.

A. VERIFICATION OF THE RESULTS OBTAINED FOR THE AREA 1

We tested 50 points distributed on a surface 5 and 10 *mm* above the PCB area under test, using the near-field measuring system to obtain measured field values. The corresponding 50 points in the model were then determined. In the next figures, we compare the measured results with the ones calculated with the proposed model. For simplicity, we decided to display only one electric or magnetic field component at two different distances which is sufficient to present the results. Fig. 13 shows the results obtained for the electric field, 5 *mm* above the PCB. The differences between the measured (experimental) and calculated (model) results are less than 3 $dB\mu V/m$ for the electric field.

Fig. 14 shows the results obtained 10 mm above the PCB surface. The differences between the measured and calculated results are less than 3.5 $dB\mu V/m$ for the electric field.

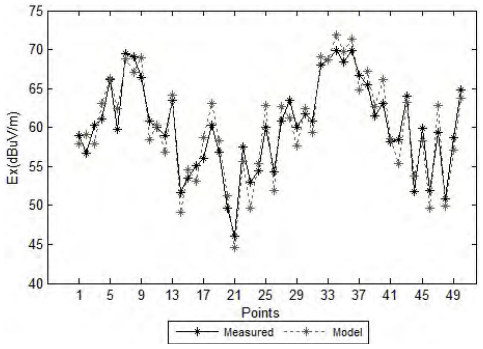

FIGURE 14. Measured and calculated results for the electric field in the area 1, 10 mm above the PCB surface.

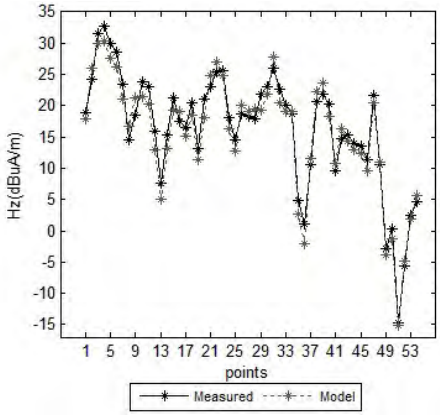

FIGURE 15. Measured and calculated results for the magnetic fields in the area 2, 10 mm over the PCB surface.

B. VERIFICATION OF THE RESULTS OBTAINED FOR THE AREA 2

For the area 2, we tested 54 points distributed on a surface 10 and 20 mm above the PCB area under test, using the near-field measuring system to obtain measured field values. The corresponding 54 points in the model were then determined. In the next figures, we compare the measured results with the ones calculated with the proposed model. Fig. 15 shows the results obtained 10 mm above the PCB. The differences between the measured and calculated results are less than 2 $dB\mu V/m$ for the magnetic field.

Fig. 16 shows the results obtained 20 mm above the PCB. The differences between the measured and calculated results are less than 3 $dB\mu V/m$ for the magnetic field.

By comparing the results obtained from the proposed model with the near-field measurement results, we conclude that the combination of the equivalent dipole model with the FDTD method was capable of effectively simulating the electromagnetic emissions radiated by the PCB under working conditions, while generating the six-channel PWM signal. There were some differences between the results obtained with the equivalent electric dipole model and the experimentally obtained results both in ordinary conditions and in the anechoic chamber (the tests in the anechoic chamber

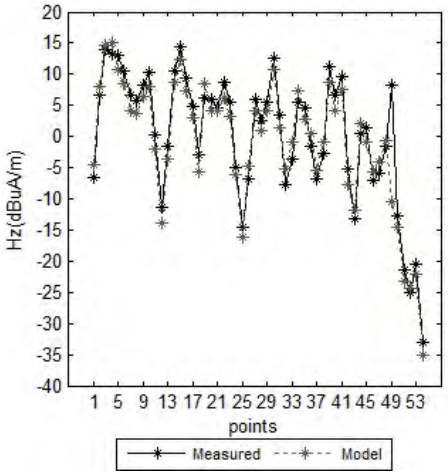

FIGURE 16. Measured and calculated results for the magnetic field in the area 2, 20 mm over the PCB surface.

will be discussed below); these differences were due to time signal errors, the limitations of the scanning area, the probe resolution, and the sampling rate of the measuring equipment.

The reason why the differences obtained for the electric field (as shown in Fig. 13 and 14) are greater than the ones obtained for the magnetic field (as shown in Fig. 15 and 16) can be described as follows:

This method requires a discretization of the electromagnetic field. (In this paper, the calculation space is discretized by Yee cells.) Both the stability conditions and the numerical dispersion conditions have been satisfied at the parameter setup stage. Nevertheless, this approach still introduces inevitable numerical errors. Furthermore, measurement errors introduce an additional difference between the real and measured values of the electric field. Therefore, the difference between the measured value of the electric field and the electric field calculated by the proposed equivalent dipole model can be considered as the combined effect of the measurement and discretization errors. In contrast, the difference between the magnetic field calculated by the model and that determined by the measured electric field results only from the model calculation error. As a result, the differences obtained for the electric field are systematically greater than the ones of the magnetic field.

C. VERIFICATION OF THE CALCULATION RESULTS USING AN ANECHOIC CHAMBER

To further verify the correctness of the proposed method, we tested the same PCB in an anechoic chamber. Different testing heights were defined, according to different test requirements.

The PCB under test was placed in an anechoic chamber. Two areas were tested, at different test heights. Fig. 17 shows the anechoic chamber testing environment. It should be noted that, to avoid the effects of other factors (such as different working conditions), the PCB was kept under the same working conditions used in the ordinary testing environment.

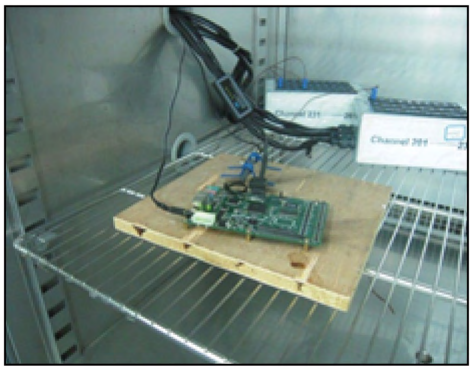

FIGURE 17. Testing environment in the anechoic chamber.

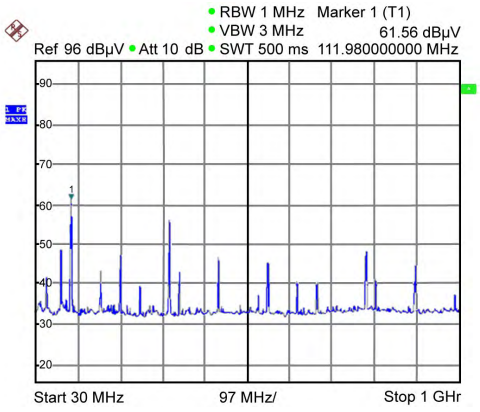

FIGURE 18. Results obtained for the area 1 of the PCB under test in the anechoic chamber, 5 mm above the PCB surface.

The first test was performed in the first test area, 5 mm above the PCB. Fig. 18 shows the obtained results. The electromagnetic radiation of the PCB under test reached its peak at 111.48 MHz, which is nearly the same value obtained in the previous tests (without the anechoic chamber). The radiation value was 61.56 $dB\mu V(U_{radition})$ in the standard laboratory testing, the cable loss was 3 $dB(L_{loss})$, and the antenna factor was 20 $dB(R_{probe})$. The test result obtained in the anechoic chamber was expressed as a voltage, and (16) was used to write the voltage in the form of an electric field. The result was 84.56 $dB\mu V/m$, and the difference between the equivalent modeling result and the measured test result was 1.44 $dB\mu V/m$. The small difference observed between the two results verifies the correctness and accuracy of the proposed method.

The test height was then increased to 10 mm for the area 1 under test. Fig. 19 shows the obtained test results. The electromagnetic radiation of the PCB under test reached its peak (52.10 $dB\mu V$) at 111.5 MHz. Using (16) to write the voltage in the form of an electric field, we obtained 75.10 $dB\mu V/m$. The difference between the equivalent model result and the test result was 2.17 $dB\mu V/m$. This small difference between the two results verifies the correctness and accuracy of this method.

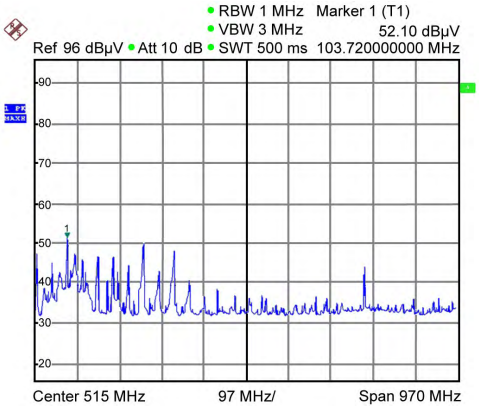

FIGURE 19. Results obtained for the area 1 of the PCB under test in the anechoic chamber, 10 mm above the PCB surface.

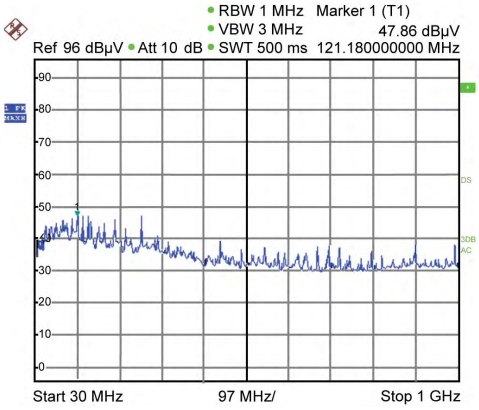

FIGURE 20. Results obtained for the area 2 of the PCB under test in the anechoic chamber, 10 mm above the PCB surface.

Subsequently, we tested the second area at a testing height of 10 mm. Fig. 20 shows the obtained results. The electromagnetic radiation of the PCB under test reached its peak at 121.18 MHz, with a value of 47.86 $dB\mu V$. Using (16) to write the voltage in the form of an electric field, a value of 70.86 $dB\mu V/m$ was obtained. The difference between the equivalent model result and the test result was 1.56 $dB\mu V/m$. Once again, the small difference obtained between the two results demonstrates the correctness and accuracy of this method.

The same area was tested again, but this time at a testing height of 20 mm. Fig. 21 shows the obtained results. The electromagnetic radiation of the PCB under test reached its peak at 121.18 MHz, with a value of 35.11 $dB\mu V$. Using (16) to write the voltage in the form of an electric field, we obtained a value of 58.11 $dB\mu V/m$. The difference between the equivalent model result and the test result was of only 1.15 $dB\mu V/m$, demonstrating again the correctness and accuracy of the proposed method.

Fig. 20 and Fig. 21 show that the differences between the measured and calculated fields decrease when the testing height increases. Generally speaking, there exists some

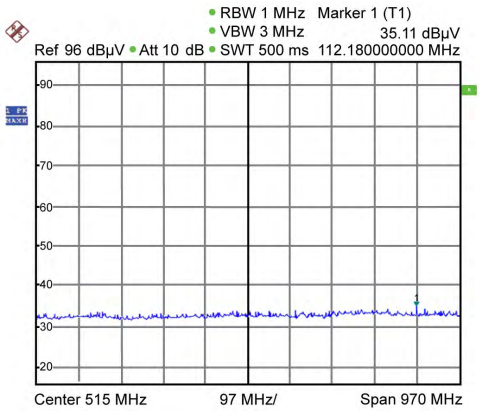

FIGURE 21. Results obtained for the area 2 of the PCB under test in the anechoic chamber, 20 mm above the PCB surface.

uncertainty in the measurements resulting from the different sets of environment in the anechoic chamber. Consequently, the difference in the measurement error between different heights results from the test environment, and is not correlated to the contents of this paper.

The above-presented experimental results show that in all cases the calculated results were a good match to the measured results, which demonstrates the correctness and accuracy of the proposed method.

V. CONCLUSION

In this study, we proposed a novel hybrid prediction method based on an equivalent dipole model and an FDTD approach to simulate the electromagnetic emission of PCBs, and therefore predict their EMC characteristics. An equivalent dipole array placed on a perfect electrically conducting plane was obtained, and shown to be capable of representing the PCB under test. To calculate the EML produced by the equivalent dipole model we constructed a calculation space using the FDTD algorithm with UPML boundary conditions.

We used magnetic dipole arrays deduced from the tangential magnetic field component. Near-field scanning at a certain height above the PCB surface was performed, and the ground plane was directly included into the equivalent model, to account for fringe effects.

We chose two test areas on a four-layer PCB; these areas contained different modules of the PCB (a digital module, and a power module). The PCB under test is therefore a representative PCB sample, and was easily modeled. The calculated and measured results in both an ordinary testing environment and an anechoic chamber were in close agreement. Therefore, the method proposed in this study can be widely used in the prediction of different types of circuit modules. Furthermore, we can apply this approach to the prediction of the electromagnetic emissions of larger, more complex circuits. The developed theory can provide useful guidance in predicting the occurrence of electromagnetic interference, and can be used to locate interference sources on the PCB.

REFERENCES

[1] Q. I. Dai, Y. H. Lo, W. C. Chew, Y. G. Liu, and L. J. Jiang, "Generalized modal expansion and reduced modal representation of 3-D electromagnetic fields," *IEEE Trans. Antennas Propag.*, vol. 62, no. 2, pp. 783–793, Feb. 2014.

[2] Z. T. Yao and J. J. Ge, "Electromagnetic compatibility of PCB based on electromagnetic simulation methods," *Appl. Mech. Mater.*, vols. 556–562, pp. 1794–1797, May 2014.

[3] P. Li and L. J. Jiang, "Source reconstruction method-based radiated emission characterization for PCBs," *IEEE Trans. Electromagn. Compat.*, vol. 55, no. 5, pp. 933–940, Oct. 2013.

[4] Z. Yu, J. A. Mix, S. Sajuyigbe, K. P. Slattery, and J. Fan, "An improved dipole-moment model based on near-field scanning for characterizing near-field coupling and far-field radiation from an IC," *IEEE Trans. Electromagn. Compat.*, vol. 55, no. 1, pp. 97–108, Feb. 2013.

[5] W. Kong and E.-P. Li, "Prediction of PCB radiated emission in shielding cavity using equivalent dipole modeling," in *Proc. IEEE Int. Symp. Electromagn. Compat. (EMC)*, Aug. 2015, pp. 1484–1488.

[6] Y. Vives-Gilabert, C. Arcambal, A. Louis, F. D. Daran, P. Eudeline, and B. Mazari, "Modeling magnetic radiations of electronic circuits using near-field scanning method," *IEEE Trans. Electromagn. Compat.*, vol. 49, no. 2, pp. 391–400, May 2007.

[7] D. W. P. Thomas, C. Smartt, and S. Greedy, "Characterisation of radiated fields from pcbs in the time domain," in *Proc. IEEE Int. Symp. Electromagn. Compat. (EMC)*, Aug. 2015, pp. 947–952.

[8] B. Ravelo, Y. Liu, and A. K. Jastrzebski, "PCB near-field transient emission time-domain model," *IEEE Trans. Electromagn. Compat.*, vol. 57, no. 6, pp. 1320–1328, Dec. 2015.

[9] X. Tong, D. W. P. Thomas, A. Nothofer, P. Sewell, and C. Christopoulos, "Modeling electromagnetic emissions from printed circuit boards in closed environments using equivalent dipoles," *IEEE Trans. Electromagn. Compat.*, vol. 52, no. 2, pp. 462–470, May 2010.

[10] L. Li *et al.*, "Measurement validation for radio-frequency interference estimation by reciprocity theorem," in *Proc. IEEE Int. Symp. Electromagn. Compat. (EMC)*, Aug. 2015, pp. 154–159.

[11] Y.-F. Mao, B. Chen, J.-L. Xia, J. Chen, and J.-Z. Tang, "Application of the leapfrog ADI FDTD method to periodic structures," *IEEE Antennas Wireless Propag. Lett.*, vol. 12, pp. 599–602, 2013.

[12] X. H. Wang, W. Y. Yin, and Z. D. Chen, "One-step leapfrog ADI-FDTD with CPML for general orthogonal grids," *IEEE Antennas Wireless Propag. Lett.*, vol. 13, pp. 1644–1647, 2014.

[13] A. K. Saxena and K. V. Srivastava, "A three-dimensional unconditionally stable five-step LOD-FDTD method," *IEEE Trans. Antennas Propag.*, vol. 62, no. 3, pp. 1321–1329, Mar. 2014.

[14] T. H. Gan and E. L. Tan, "Unconditionally stable fundamental LOD-FDTD method with second-order temporal accuracy and complying divergence," *IEEE Trans. Antennas Propag.*, vol. 61, no. 5, pp. 2630–2638, May 2013.

[15] H. Li, H. Zhou, Y. Liu, X. Bao, and Z. Zhao, "Massively parallel FDTD program JEMS-FDTD and its applications in platform coupling simulation," in *Proc. Int. Symp. Electromagn. Compat.*, Sep. 2014, pp. 229–233.

[16] Z.-Y. Huang, L.-H. Shi, Y. Zhou, and B. Chen, "UPML-ABC and TF/SF boundary for unconditionally stable AH-FDTD method in conductive medium," *Electron. Lett.*, vol. 51, no. 21, pp. 1654–1656, Oct. 2015.

[17] I. Giannakis and A. Giannopoulos, "Time-synchronized convolutional perfectly matched layer for improved absorbing performance in FDTD," *IEEE Antennas Wireless Propag. Lett.*, vol. 14, pp. 690–693, 2015.

[18] Y. Yu and Z. Chen, "The CPML absorbing boundary conditions for the unconditionally stable meshless modeling," *IEEE Antennas Wireless Propag. Lett.*, vol. 11, pp. 468–472, 2012.

[19] T. Hikage, Y. Kawamura, and T. Nojima, "Numerical estimation methodology for RFID/active implantable medical device-EMI based upon FDTD analysis," in *Proc. 30th Gen. Assembly Sci. Symp. (URSI)*, Aug. 2011, pp. 1–4.

[20] Z. Ye, C. Liao, X. Xiong, and M. Zhang, "The research and application of a novel time domain hybrid method for EMI analysis of lumped circuits in a shielded device," *IEEE Trans. Electromagn. Compat.*, vol. 58, no. 4, pp. 964–970, Aug. 2016.

[21] D. Yan, L. Sun, Y. Sun, and B. Jiang, "The FDTD analysis of EMI in motor drive system," in *Proc. 6th World Congr. Intell. Control Autom. (WCICA)*, Jun. 2006, pp. 8074–8078.

[22] D. Baudry, C. Arcambal, A. Louis, B. Mazari, and P. Eudeline, "Applications of the near-field techniques in EMC investigations," *IEEE Trans. Electromagn. Compat.*, vol. 49, no. 3, pp. 485–493, Aug. 2007.

LANYONG ZHANG (M'15) received the Ph.D. degree in theory and control engineering in 2011. In 2009, he received the Excellent Graduate Award from the same university. His current research interests include the fast transient analysis and modeling of field-excited multiconductor networks, power-line carrier propagation, electromagnetic field interference from overhead multiconductor lines, and electromagnetic interaction with advanced composite materials.

He is currently a master's Supervisor with Harbin Engineering University. His main tutorial research interests are electromagnetic compatibility prediction and measurement and stochastic signal processing.

LEI ZHANG (M'17) was born in Dezhou, China, in 1992. He received the B.S. degree in automation from the Shandong University of Science and Technology. He is currently pursuing the M.S. degree in control science and engineering with Harbin Engineering University, Harbin, China. He is a Volunteer of the IEEE computer society in 2017.

BANGMIN WANG received the B.S. degree from Harbin Engineering University in 2014, where he is currently pursuing the Ph.D. degree in electromagnetic compatibility prediction measurement and electromagnetic compatibility signal processing.

SHENG LIU was born in Baicheng, China, in 1957. He received the B.Eng. degree in industrial automation from the Harbin University of Civil Engineering and Architecture, Harbin, China, in 1982, and the master's and Ph.D. degrees in theory and control engineering from Harbin Engineering University, Harbin, in 1982 and 2000, respectively. He is currently a Professor with Harbin Engineering University. His current research interests include electromagnetic compatibility prediction and measurement, optimization estimate and control of random system, and robust control and ship control system.

CHRISTOS PAPAVASSILIOU (M'96–SM'05) was born in Athens, Greece, in 1960. He received the B.Sc. degree in physics from the Massachusetts Institute of Technology, Cambridge, MA, USA, and the Ph.D. degree in applied physics from Yale University, New Haven, CT, USA.

He has researched on GaAs monolithic microwave integrated circuit (MMIC) design and measurements with the Foundation for Research and Technology, Hellas, Crete, Greece, and was involved in several European and regional projects on GaAs MMIC technology. Since 1996, he has been with Imperial College London, where he has involved in SiGe technology development, RF IC, and instrumentation. He has contributed to over 70 publications. His current research interests include memristor applications, electromagnetic surface wave propagation oninterfaces, and antenna.